Supplementary Information

Local ionic transport enables selective PGM-free bipolar membrane electrode assembly

Mengran Li[1,2,*, £], Eric W. Lees[3, 4, £], Wen Ju[5,6, £], Siddhartha Subramanian[1], Kailun Yang[1], Justin C. Bui[7, 8], Hugo-Pieter Iglesias van Montfort[1], Maryam Abdinejad[1, 9], Joost Middelkoop[1], Peter Strasser[5], Adam Z. Weber[3], Alexis T. Bell[7,8], Thomas Burdyny[1,*]

1. Department of Chemical Engineering, Delft University of Technology; 9 van der Maasweg, Delft, 2629HZ, the Netherlands
2. Department of Chemical Engineering, the University of Melbourne, Melbourne, Victoria, 3010, Australia
3. Energy Technologies Area, Lawrence Berkeley National Laboratory, Berkeley, CA 94720, USA
4. Department of Chemical and Biological Engineering, The University of British Columbia, 2360 East Mall, Vancouver, British Columbia, V6T 1Z3, Canada.
5. Chemical Engineering Division, Department of Chemistry, Technical University Berlin, Berlin, Germany
6. Department of Electrochemistry and Catalysis, Leibniz Institute for Catalysis, 18059, Rostock, Germany
7. Chemical Sciences Division, Lawrence Berkeley National Laboratory, Berkeley, CA 94720, USA
8. Department of Chemical and Biological Engineering, University of California Berkeley, Berkeley, CA 94720, USA
9. Department of Chemical Engineering, Massachusetts Institute of Technology, Cambridge, MA 02139 USA

£ M. Li, E. W. Lees, and J. Wen contributed equally to this work.

*Correspondence to:

M. Li: aaron.li1@unimelb.edu.au

T. Burdyny: t.e.burdyny@tudelft.nl

Theory and model development

A 1D isothermal continuum model was developed for the cation exchange layer (CEL) and catalyst layer (CL) of the BPM-based CO_2 electrolyser MEA based on previous porous electrode models by Weng *et al.*[1] and Lees *et al.*[2] (Fig. S1). The CL domain of the model was assumed to be composed of gas, Sustainion ionomer, and solid NiNC-IMI catalyst phases with constant volume fractions of 0.37, 0.43, and 0.2, respectively. These values correspond to the volume fractions of the ionomer and catalyst in the ink precursor. The CEL domain was assumed to be impermeable to gas transport and composed entirely of Sustainion ionomer.

Governing equations

The current density (i_s) and potential (ϕ_s) profiles in the solid-fraction of the catalyst layer were determined using Ohm's law,

$$i_s = -\nabla \cdot (\sigma_{\text{eff}}\phi_s) \qquad \text{Eq. S1}$$

where the effective conductivity (σ_{eff}) is estimated based on the nominal conductivity of solid silver σ_s using the Bruggeman relation,

$$\sigma_{\text{eff}} = \varepsilon_S^{1.5}\sigma_s \qquad \text{Eq. S2}$$

Steady-state continuity equations were used to determine the flux (n) of each chemical species j in the gas-phase ($j = CO_{2(g)}$, $CO_{(g)}$, $H_{2(g)}$, and $H_2O_{(g)}$) and i in the ionomer-phase species i ($i = H^+_{(aq)}$, $OH^-_{(aq)}$, $HCO_3^-_{(aq)}$, $CO_3^{2-}_{(aq)}$, and $K^+_{(aq)}$),

$$\nabla \cdot n_j = \varepsilon_G \sum_j R_{k,j} \qquad \text{Eq. S3}$$

$$\nabla \cdot n_i = \varepsilon_I \sum_i R_{k,i} \qquad \text{Eq. S4}$$

where ε_G is the gas-volume fraction in the CL, ε_I is the volume fraction of ionomer in the catalyst layer, and $R_{k,i}$ is the volumetric rate of generation/consumption by process k of species j or i. The gas-phase fluxes (n_j) were determined using a system of Stefan-Maxwell equations for multi-component mass transport,

$$n_j = -\rho_g D_j^{\text{eff}}\nabla\omega_j - \rho_G D_j^{\text{eff}}\omega_j\frac{\nabla M_n}{M_n} + \rho_j u_G \qquad \text{Eq. S5}$$

where ω_j is the mass fraction of species j, ρ_G is the density of the gas-phase, D_j^{eff} is the effective diffusion coefficients, M_n is the average molecular weight. The convective velocity of the gas-phase (u_G) in the CL pores was determined as follows,

$$u_G = -\frac{\kappa_{sat,CL}\kappa_{rG,CL}}{\mu_G}\nabla p_G \qquad \text{Eq. S6}$$

where μ_G is the gas viscosity, and κ_{sat}^0 is the bulk saturated permeability. The relative permeability (κ_{rG}) of the gas-phase was estimated based on the correlation given by Zenyuk *et al.*,[3]

$$\kappa_{rg,CL} = \left(1 - \frac{\varepsilon_I}{\varepsilon_G + \varepsilon_I}\right)^3 \qquad \text{Eq. S7}$$

The final equation used to solve the governing mass balances is given as,

$$\sum_j \omega_j = 1 \qquad \text{Eq. S8}$$

The flux of each chemical species in the ionomer-phase (n_i) was determined using the Nernst-Planck equation for dilute-solutions,

$$n_i = -D_i^{\text{eff}}\nabla c_i - z_i \frac{F}{RT}D_i^{\text{eff}}c_i\nabla\phi_I \qquad \text{Eq. S9}$$

where z_i is the charge of the mobile ionic species, F is Faraday's constant (96485 C/mol), R is the ideal gas constant (8.314 $\frac{J}{mol\ K}$), T is the temperature (298.15 K), and ϕ_I is the ionomer-phase potential. The charge neutrality constraint was used as the final equation to solve the governing mass balance,

$$\sum_i z_i c_i + \rho_{\text{ionomer}}\text{IEC}_{\text{ionomer}} = 0 \qquad \text{Eq. S10}$$

Where $\rho_{ionomer}$ and $\text{IEC}_{\text{ionomer}}$ are the density and ion exchange capacity of the ionomer (units: mol/g wet polymer) in either the CEL or CL.

Charge transfer and source terms

The electrochemical reactions consume reactants and generate products at the ionomer/solid interface according to Faraday's Law,

$$R_{CT,i} = -M_i \frac{a_v s_{i,k} i_k}{n_k F}$$

Eq. S11

where M_i is the molar mass of species i, a_v is the specific surface area of the catalyst layer, $s_{i,k}$ is the stoichiometric coefficient for species i in reaction k. We considered the specific surface area (a_v) to be the interfacial area between the ionomer and solid Ni portions of the CL as follows,

$$a_v = \frac{\varepsilon_I}{\varepsilon_G + \varepsilon_I} a_v^0$$

Eq. S11

where a_v^0 is the specific surface area of the catalyst without ionomer. The kinetics of the electrochemical reactions are governed by concentration-dependent Butler-Volmer kinetics as given by as per Weng *et al.*,[1]

$$i_{CO} = -i_{0,CO} \left(\frac{c_{CO_2}}{1\,M} \right)^{1.5} exp \left(-\frac{\alpha_{c,CO} F}{RT} \eta_{CO} \right)$$

Eq. S12

$$i_{H_2} = -i_{0,H_2} \left(-\frac{\alpha_{c,HER} F}{RT} \eta_{HER} \right)$$

Eq. S13

Where $i_{0,CO2R}$ and i_{0,H_2} are the exchange current densities for the CO2-to-CO reaction and hydrogen evolution reaction (HER), respectively. $\alpha_{c,HER}$ and $\alpha_{c,CO}$ are the transfer coefficients for the HER and CO2R, respectively. The pH-dependent kinetics of the HER are given by Weng *et al.*,[4]

$$i_{0,H_2} = A_{HER} exp \left(-\frac{(83 + pH) \left[\frac{kJ}{mol} \right]}{RT} \right)$$

Eq. S14

Where A_{HER} is the collision frequency for the HER. The overpotential of electrochemical reaction k was determined based on the standard reduction potential (U_k^0) and the pH according to the Nernst equation,

$$\eta_k = \phi_s - \phi_l - \left(U_k^0 - \frac{2.303 RT}{F} pH \right)$$

Eq. S15

The source terms associated with the acid-base reactions in the ionomer were determined as,

$$R_{B,i} = M_i \sum_i s_{i,n} (k_n \prod_{s_{i,n} < 0} c_i^{-s_{i,n}} - \frac{k_n}{K_n} \prod_{s_{i,n} > 0} c_i^{s_{i,n}})$$

Eq. S16

where K_n is the equilibrium constant of homogeneous reaction n, $s_{i,n}$ is the stoichiometric coefficient of species i in homogeneous bulk reaction n ($s_{i,n} < 0$ for reactants and $s_{i,n} > 0$ for products). k_n and k_{-n} are the forward and reverse reaction rate constants for reaction n, respectively. The phase-transfer term for CO_2 at the gas-ionomer interface was calculated using a mass transfer correlation,

$$R_{PT,CO_2} = a_v k_{GL,CO_2} M_{CO_2} \left(H_{CO_2} p_g y_{CO_2} - c_{CO_2} \right)$$

Eq. S17

where H_{CO_2} is the Henry's Law coefficient for CO_2 dissolved in water, y_{CO_2} is the mole fraction of CO_2 in the gas-phase, and k_{GL,CO_2} is the mass transfer coefficient for CO_2 through the ionomer film on the catalyst surface,

$$k_{GL,CO_2} = \frac{D_{CO_2,w}}{\delta_{DL}}$$

Eq. S18

where $D_{CO_2,w}$ is the diffusion coefficient of CO_2 in water and δ_{DL} is the diffusion boundary layer thickness. This value was estimated based on the pore structure and volume fraction of ionomer as per Weng *et al.*,[1]

$$\delta_{TF} = r_{CL} \left(1 - \sqrt{1 - \frac{\varepsilon_I}{\varepsilon_G + \varepsilon_I}} \right)$$

Eq. S19

CO and H_2 were assumed to be insoluble in the ionomer and therefore the rate of CO and H generation gas-phase were also calculated by Faraday's Law,

$$R_{PT,j} = -M_i \frac{a_v s_{j,k} i_k}{n_k F}$$

Eq. S20

Effective diffusion coefficients

The effective diffusion coefficients for the gas-phase species (D_j^{eff}) were determined by considering the molecular and Knudsen diffusivities as parallel resistances as follows,

$$D_j^{eff} = \left(\frac{1}{D_j^m} + \frac{1}{D_j^K} \right)^{-1}$$

Eq. S21

$$D_j^m = \frac{1 - \omega_j}{\sum_{b \neq j} \frac{y_b}{D_{j,b}}}$$

Eq. S22

$$D_j^K = \frac{2r_{pore}}{3}\sqrt{\frac{8RT}{\pi M_j}} \qquad \text{Eq. S23}$$

Where D_j^m and D_j^K are the mass-averaged molecular and Knudsen diffusion coefficients, respectively, of species j. r_{pore} is the CL pore radius and y_b is the mole fraction of another component gas b. $D_{j,b}$ is the diffusivity of species j in species b, which was estimated based on the Fuller method.[5]

The effective diffusion coefficients for the chemical species in the ionomer-phase (D_i^{eff}) were determined based on the porosity and hydration (λ) of the ionomer as per Grew *et al.*[6] These equations considers ion transport through the water-filled pore volume of the ionomer (Φ),

$$D_i^{eff} = \frac{\Phi^{q_i}D_{i,w}}{x_w(1+\psi_i)} \qquad \text{Eq. S24}$$

$$\Phi = \frac{\lambda V_W}{\lambda V_W + V_M} \qquad \text{Eq. S25}$$

$$x_w = \frac{\lambda}{\lambda + 1} \qquad \text{Eq. S26}$$

ψ_i is the ratio between species-solvent and species-membrane interaction effects, which is defined based on the reduced molecular weight of species i in the membrane ($M_{i,M}$) and in water ($M_{i,w}$),

$$\psi_i = \frac{1}{\lambda}\left(\frac{V_M}{V_w}\right)^{\frac{2}{3}}\left(\frac{M_{i,M}}{M_{i,w}}\right)^{\frac{1}{2}} \qquad \text{Eq. S27}$$

$$M_{i,M} = \left(\frac{1}{M_i} + \frac{1}{M_M}\right)^{-1} \qquad \text{Eq. S28}$$

$$M_{i,w} = \left(\frac{1}{M_i} + \frac{1}{M_w}\right)^{-1} \qquad \text{Eq. S29}$$

where V_w is the molar volume of water and the molecular weight of the membrane (M_M) is estimated as 10,000 g mol^{-1}. The molar volume of the membrane (V_M) was calculated based on the ion exchange capacity (IEC) and the density of the ionomer ($\rho_{ionomer}$),

$$V_M = \frac{1}{\rho_{ionomer}IEC} \qquad \text{Eq. S30}$$

q_i is a tortuosity parameter set to values of 1.5 for co-ion transport (e.g., CO_3^{2-} transport in the cation exchange ionomer of the CEL) and 1 for counter-ion transport (e.g., OH^- transport in the Sustainion ionomer of the CL) . V_W is the molar volume of water, V_M is the molar volume of water in the polymer, and x_w is the mole fraction of water in the ionomer.

The hydration of the CEL ionomer λ_{CEL} was estimated by interpolating between the experimentally-measured values for the CEL of a BPM in K^+ and H^+ forms as per Bui $et\ al.$,[7]

$$\lambda_{CEL} = \lambda_{x_{H^+}=0} + x_{H^+}\lambda_{x_{H^+}=1} \qquad \text{Eq. S31}$$

where $\lambda_{x_{H^+}=0} = 6$ and $\lambda_{x_{H^+}=1} = 9$ are the hydration values obtained from fitting experimental electrodialysis data[6] and x_{H^+} is the fraction of negatively-charged groups in the CEL that are charge-balanced by H^+,

$$x_{H^+} = \frac{c_{H^+}}{\rho_{CEL}IEC_{CEL}} \qquad \text{Eq. S32}$$

The hydration value of the Sustainion ionomer ($\lambda_{Sustainion}$) was calculated by interpolating the values measured by Luo $et\ al.$[8] for CO_3^{2-} and OH^- forms of Sustainion at 100% relative humidity,

$$\lambda_{Sustainion} = \lambda_{x_{CO_3^{2-}}=0} + x_{CO_3^{2-}}\lambda_{x_{CO_3^{2-}}=1} \qquad \text{Eq. S33}$$

Where $x_{CO_3^{2-}}$ is given as,

$$x_{CO_3^{2-}} = \frac{c_{CO_3^{2-}}}{\rho_{AEL}IEC_{AEL}} \qquad \text{Eq. S34}$$

Boundary conditions and Donnan equilibrium

The 1D model domain is shown in Figure S1. The water dissociation interface of the BPM exists at the left-hand side of the model domain. At this interface, the ionic fluxes were defined based on the transference number for H^+ (t_{H_+}) as per Lees *et al.*,[6]

$$n_{H^+}|_{x=0} = -t_{H^+} \int_{x=L_{CEL}}^{x=L_{CEL}+L_{CL}} \frac{(i_{CO} + i_{H_2})}{n_{WD}F} dx \qquad \text{Eq. S35}$$

$$n_{K^+}|_{x=0} = -(1 - t_{H^+}) \int_{x=L_{CEL}}^{x=L_{CEL}+L_{CL}} \frac{(i_{CO} + i_{H_2})}{n_{WD}F} dx \qquad \text{Eq. S36}$$

where n_{WD} is the moles of H^+ produced by water dissociation per mole of electron passed through the circuit. The measured t_{H_+} value from the BPMEA cell experiment with 0.1 M KOH as the anolyte was used in the model. The flux of all other species in the ionomer was assumed to be 0 at the water dissociation interface, given that the titration experiment performed after electrolysis showed low carbonate crossover to the anolyte (<1% of the total charge passed),

$$n_{i \neq K^+, H^+}|_{x=0} = 0 \qquad \text{Eq. S37}$$

The reference potential for the ionomer-phase was also defined at the water dissociation interface,

$$\phi_l|_{x=0} = 0 \qquad \text{Eq. S38}$$

The potential and concentration profiles at the interface between the CEL and Sustainion ionomer in the CL were determined based on the Donnan equilibrium,

$$\phi_l|_{x=L_{CEL^-}} = \phi_l|_{x=L_{CEL^+}} - \frac{RT}{z_i F} ln\left(\frac{c_{i,x=L_{CEL^+}}}{c_{i,x=L_{CEL^-}}}\right) \qquad \text{Eq. S39}$$

where $c_{i,x=L_{CEL^+}}$ and $c_{i,x=L_{CEL^-}}$ are the concentrations of species i in the Sustainion CL ionomer and CEL membrane, respectively. A Dirichlet boundary condition was imposed on the concentration of chemical species in the ionomer at the CL/GDL interface,

$$c_i|_{x=L_{CEL}+L_{CL}} = c_i^{Bulk} \qquad \text{Eq. S40}$$

where c_i^{Bulk} is the bulk electrolyte composition corresponding to 1 M $KHCO_{3(aq)}$ under a CO_2-saturated atmosphere (pH = 7.6). The CO_2 concentration in the bulk is calculated according to Henry's Law,

$$c_{CO_2}^{Bulk} = H_{CO_2} p_g y_{CO_2}$$

<div align="right">Eq. S41</div>

The flux of chemical species j in the gas-phase was set to 0 at the CEL/CL interface and a mass transfer correlation was used to simulate the transport of CO_2, H_2O, CO, and H_2 through the gas diffusion layer,

$$n_j|_{x = L_{CEL}} = 0$$

<div align="right">Eq. S42</div>

$$n_j|_{x = L_{CEL} + L_{CL}} = -k_{MT}\left(\omega_j^{Bulk} - \omega_j|_{x=L_{CEL}+L_{CL}}\right)$$

<div align="right">Eq. S43</div>

where ω_j^{Bulk} represent the mass fraction of chemical species j in the bulk humidified CO_2 stream. $\omega_j|_{x=L_{CEL}+L_{CL}}$ is the mass fraction at the CL/GDL interface and k_{MT} is a mass transfer coefficient for a flat-plate geometry as per Weng $et\ al.$[1] The pressure at the CL/GDL interface was set to 1 atm to solve the momentum balance,

$$p_G|_{x = L_{CEL} + L_{CL}} = 1\ \text{atm}$$

<div align="right">Eq. S44</div>

Finally, the solid-phase potential at the CL/GDL interface was varied from –1.5 to –2.5 V to simulate different current densities. Table S1 below shows the pertinent parameters used in the governing equations and boundary conditions.

**Table S1: 1D continuum model parameters**

Parameter	Value	Unit	Reference (in Supplementary Information)
CL properties			
L_{CL}	10	μm	Experiment
a_v^0	1×10^7	m^{-1}	[1]
ε_G	0.37	—	Experiment
ε_I	0.43	—	Experiment
ε_S	0.20	—	Experiment
$\kappa_{sat,CL}^0$	8×10^{-16}	m^2	[1]
σ_S	100	S cm^{-1}	[1]
r_{CL}	5	μm	[2]
$\lambda_{x_{CO_3^{2-}}=1}$	11	—	[5]
$\lambda_{x_{CO_3^{2-}}=0}$	25	—	[5]
CEL properties			
L_{CEL}	75	μm	[4]
ρ_M	1	g mL^{-1}	[4]
IEC	1.81	mmol g^{-1}	[4]
$\lambda_{x_{H^+}=1}$	9	—	[4]
$\lambda_{x_{H^+}=0}$	6	—	[4]
t_{H^+}	0.99	—	Experiment
Homogeneous Reactions			
k_1	3.71×10^{-2}	s^{-1}	[1]
K_1	$10^{-6.37}$	M	[1]
k_2	59.44	s^{-1}	[1]
K_2	$10^{-10.32}$	M	[1]
k_3	2.2×10^3	L mol^{-1} s^{-1}	[1]
k_4	6.0×10^9	L mol^{-1} s^{-1}	[1]

|			
K_W	10^{-14}	M^2	1
Electrochemical Reactions			
U_{CO}^0	–0.11	V	1
$i_{0,CO}$	1.05×10^{-4}	mA cm^{-2}	Fit value
$\alpha_{c,CO}$	0.30	—	Fit value
U_{HER}^0	0	V	1
$i_{0,HER,acid}$	0.63	mA cm^{-2}	Fit value
$\alpha_{c,HER}$	0.47	—	Fit value
A_{HER}	8840	mA cm^{-2}	Fit value
Bulk concentrations in the liquid phase			
$c_{H^+}^{Bulk}$	$10^{-7.6}$	M	Equilibrium
$c_{K^+}^{Bulk}$	1	M	Electroneutrality
$c_{OH^-}^{Bulk}$	$10^{-6.4}$	M	Equilibrium
$c_{HCO_3^-}^{Bulk}$	1	M	Electroneutrality
$c_{CO_3^{2-}}^{Bulk}$	0	M	Equilibrium
Liquid phase transport			
$D_{H^+,w}$	9.31×10^{-5}	cm^2 s^{-1}	1
$D_{K^+,w}$	1.96×10^{-5}	cm^2 s^{-1}	1
$D_{OH^-,w}$	4.95×10^{-5}	cm^2 s^{-1}	1
$D_{HCO_3^-,w}$	1.19×10^{-5}	cm^2 s^{-1}	1
$D_{CO_3^{2-},w}$	0.80×10^{-5}	cm^2 s^{-1}	1
$D_{CO_2,w}$	1.66×10^{-5}	cm^2 s^{-1}	1
Bulk mass fractions for the gas phase			
ω_{CO}^{Bulk}	0	—	Inlet conditions
$\omega_{H_2}^{Bulk}$	0	—	Inlet conditions
$\omega_{CO_2}^{Bulk}$	0.779	—	Inlet conditions
$\omega_{H_2O}^{Bulk}$	0.221	—	Inlet conditions

Supplementary data
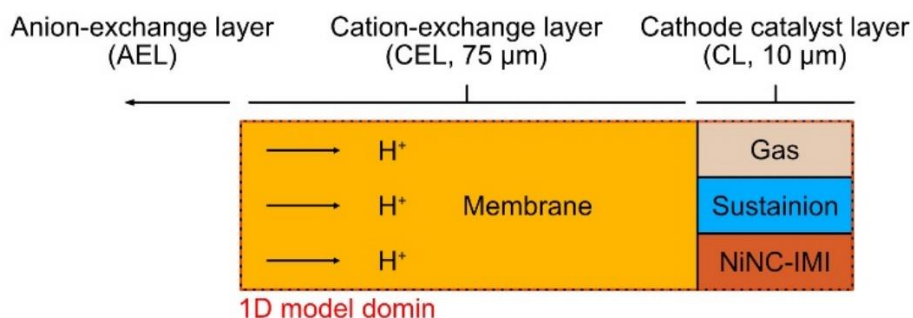
Fig. S1 Schematic diagram of 1D continuum model domains for the studied cation exchange layer (CEL) for the BPM and catalyst layer (CL) based on NiNC-IMI catalyst embedded with Sustainion ionomer.
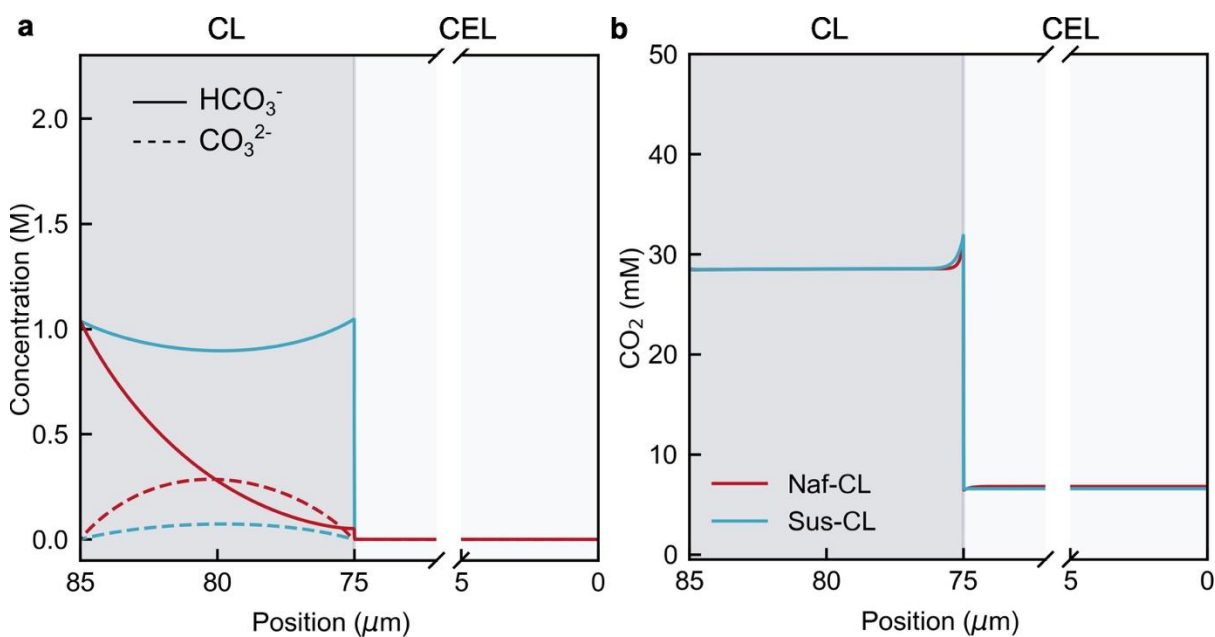

Fig. S2 Comparison of the modelled concentrations of HCO_3^-, CO_3^{2-}, and CO_2 for Naf-CLs and Sus-CLs across CL and CEL. The Naf-CLs represent the catalyst layer based with Nafion ionomer and Sus-CLs represent the ones based with Sustainion ionomer. The position between 0-75 μm is for the modelled CEL; the position between 75-85 μm is for CL.
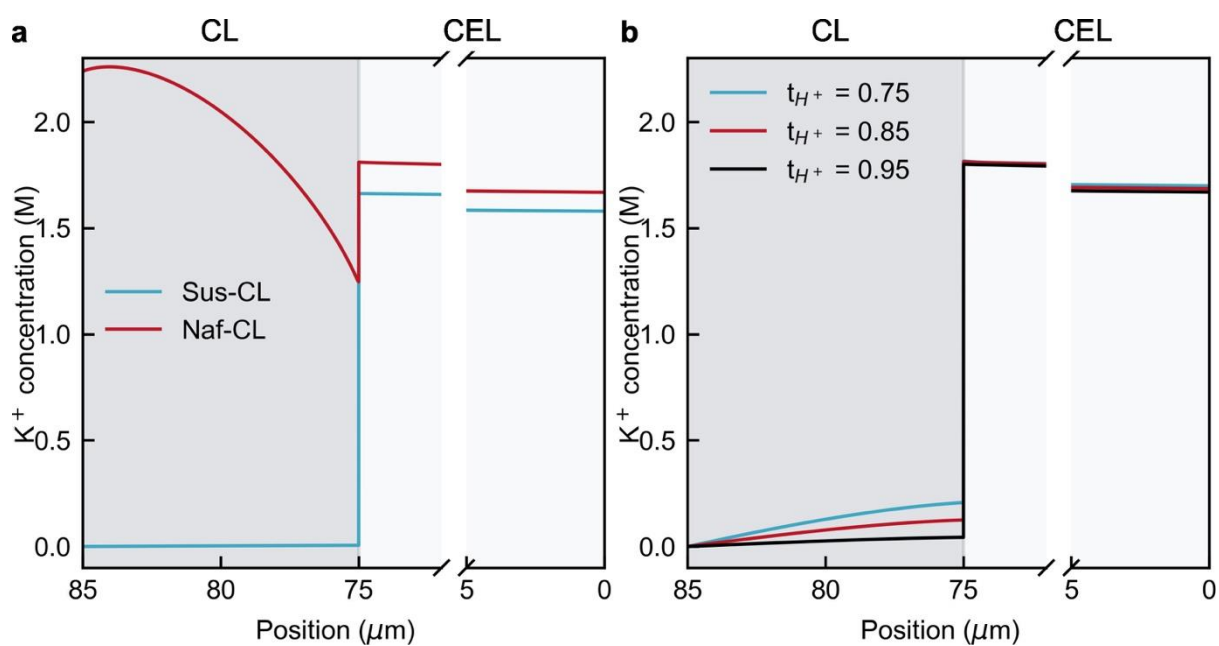
Fig. S3 Concentration profiles of K⁺ for (a) CLs based with Sustainion (Sus-CL) or Nafion (Naf-CL) ionomers and (b) proton transference numbers (denoted as t_{H^+}) across the CLs and CEL.
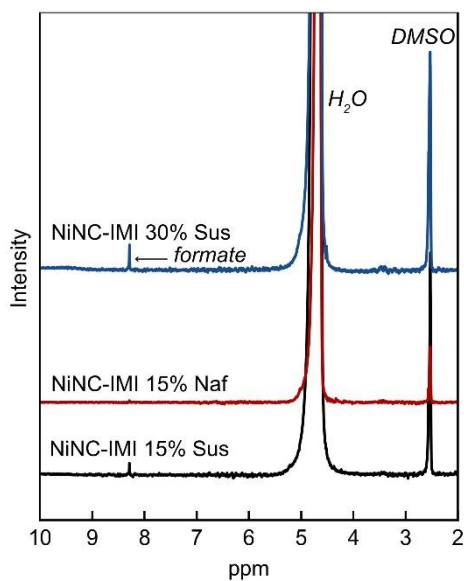
Fig. S 4 Comparison of the nuclear magnetic resonance spectroscopy results for anolytes after CO_2 electrolysis performance test of BPMEAs with different CLs based on 30% Sustainion ionomer (NiNC-IMI 30% Sus), 15% Nafion ionomer (NiNC-IMI 15% Naf), and 15% Sustainion ionomer (NiNC-IMI 15%). Dimethyl sulfoxide (DMSO) is the internal reference to quantify the liquid products (*i.e.*, formate in this study) produced from CO_2 electroreduction and transported to the anolyte.
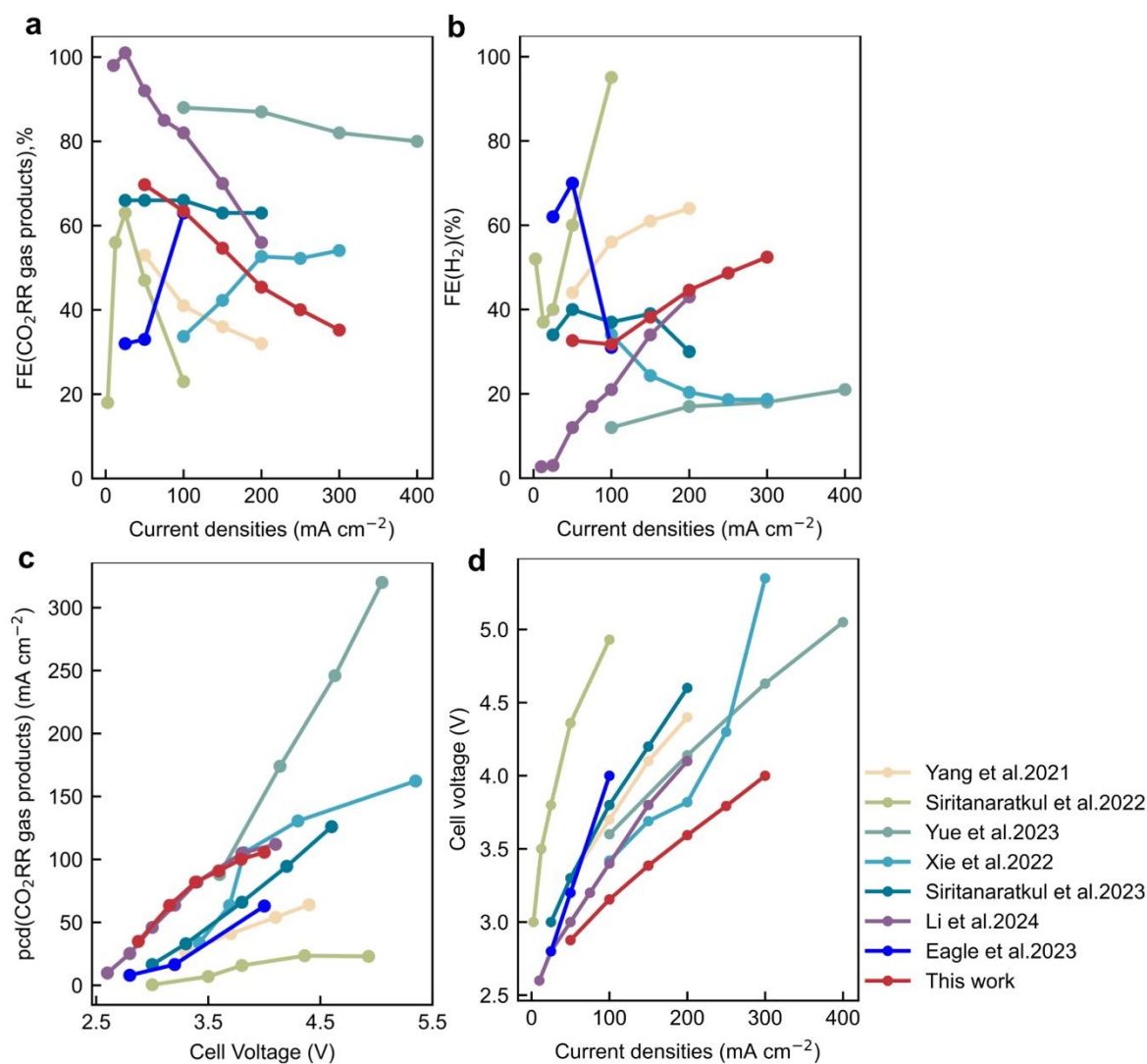
Fig. S5 Performance comparison with literature data. Comparison of (a) FEs for CO₂ reduction reaction (CO₂RR) gaseous products, (b) FEs for H₂, (c) partial current density of CO₂RR gaseous product, and (d) cell voltages of BPMEA with NiNC-IMI 15% Sus CL as cathode with recently reported literature data by Yang et al.[9], Siritanaratkul et al.[10,11], Yue et al.[12], Xie et al.[13], Li et al.[14], and Eagle et al.[15].

Table S 1 Summary of the literature data for comparison.

| Current density (mA cm-2)	FE(CO2 RR, gas),%	FE(H2), %	Cell voltages, V	Cathode	Cathode ionomer	Membrane	Anode	Anolyte	Gas product	Remarks	Refs
50	53	44	3.3	100 nm sputtered Ag @ Sigracet 39BC	N.A.	Fumasep FBM	Ni Foam	1M KOH	CO	N.A.	Yang et al.2021[9]
100	41	56	3.7	100 nm sputtered Ag @ Sigracet 39BC	N.A.	Fumasep FBM	Ni Foam	1M KOH	CO	N.A.	Yang et al.2021[9]
150	36	61	4.1	100 nm sputtered Ag @ Sigracet 39BC	N.A.	Fumasep FBM	Ni Foam	1M KOH	CO	N.A.	Yang et al.2021[9]
200	32	64	4.4	100 nm sputtered Ag @ Sigracet 39BC	N.A.	Fumasep FBM	Ni Foam	1M KOH	CO	N.A.	Yang et al.2021[9]
2.5	18	52	3	[Ni(Cyc)]2+ @Sigracet 39BC	Nafion	Fumasep FBM	RuO2 coated Sigracet 39BC	H2O	CO	N.A.	Siritanaratkul et al.2022[14]
12.5	56	37	3.5	[Ni(Cyc)]2+ @Sigracet 39BC	Nafion	Fumasep FBM	RuO2 coated Sigracet 39BC	H2O	CO	N.A.	Siritanaratkul et al.2022[14]
25	63	40	3.8	[Ni(Cyc)]2+ @Sigracet 39BC	Nafion	Fumasep FBM	RuO2 coated Sigracet 39BC	H2O	CO	N.A.	Siritanaratkul et al.2022[14]
50	47	60	4.36	[Ni(Cyc)]2+ @Sigracet 39BC	Nafion	Fumasep FBM	RuO2 coated Sigracet 39BC	H2O	CO	N.A.	Siritanaratkul et al.2022[14]
100	23	95.07	4.93	[Ni(Cyc)]2+ @Sigracet 39BC	Nafion	Fumasep FBM	RuO2 coated Sigracet 39BC	H2O	CO	N.A.	Siritanaratkul et al.2022[14]
100	88	12	3.6	0.5 mg cm-2 Ni SAC@ Freudenberg H14C9	Nafion	Fumasep FBM	Ni Foam	1M KOH	CO	23wt% Nafion compared to catalyst loading in the catalyst layer	Yue et al.2023[12]
200	87	17	4.14	0.5 mg cm-2 Ni SAC@ Freudenberg H14C10	Nafion	Fumasep FBM	Ni Foam	1M KOH	CO	23wt% Nafion compared to catalyst loading in the catalyst layer	Yue et al.2023[12]
300	82	18	4.63	0.5 mg cm-2 Ni SAC@ Freudenberg H14C11	Nafion	Fumasep FBM	Ni Foam	1M KOH	CO	23wt% Nafion compared to catalyst loading in the catalyst layer	Yue et al.2023[12]
400	80	21	5.05	0.5 mg cm-2 Ni SAC@ Freudenberg H14C12	Nafion	Fumasep FBM	Ni Foam	1M KOH	CO	23wt% Nafion compared to catalyst loading in the catalyst layer	Yue et al.2023[12]
100	34	34	3.42	1 mg cm-2 Cu NP on carbon paper	Nafion	Fumasep FBM			CO, C2H4	65 um stationary catholyte layer	Xie et al.2022[13]

| 150	42	24	3.69	1 mg cm-2 Cu NP on carbon paper	Nafion	Fumasep FBM	IrO2 loaded Ti felt	0.1M KHCO3	CO, C2H4	65 um stationary catholyte layer	Xie et al.2022[13]
200	53	20	3.82	1 mg cm-2 Cu NP on carbon paper	Nafion	Fumasep FBM	IrO2 loaded Ti felt	0.1M KHCO3	CO, C2H4	65 um stationary catholyte layer	Xie et al.2022[13]
250	52	19	4.3	1 mg cm-2 Cu NP on carbon paper	Nafion	Fumasep FBM	IrO2 loaded Ti felt	0.1M KHCO3	CO, C2H4	65 um stationary catholyte layer	Xie et al.2022[13]
300	54	19	5.35	1 mg cm-2 Cu NP on carbon paper	Nafion	Fumasep FBM	IrO2 loaded Ti felt	0.1M KHCO3	CO, C2H4	65 um stationary catholyte layer	Xie et al.2022[13]
25	66	34	3	CoPc/C on carbon paper	Nafion	Fumasep FBM	RuO2 loaded on carbon paper	1M KOH	CO	N.A.	Siritanaratkul et al.2023[15]
50	66	40	3.3	CoPc/C on carbon paper	Nafion	Fumasep FBM	RuO2 loaded on carbon paper	1M KOH	CO	N.A.	Siritanaratkul et al.2023[15]
100	66	37	3.8	CoPc/C on carbon paper	Nafion	Fumasep FBM	RuO2 loaded on carbon paper	1M KOH	CO	N.A.	Siritanaratkul et al.2023[15]
150	63	39	4.2	CoPc/C on carbon paper	Nafion	Fumasep FBM	RuO2 loaded on carbon paper	1M KOH	CO	N.A.	Siritanaratkul et al.2023[15]
200	63	30	4.6	CoPc/C on carbon paper	Nafion	Fumasep FBM	RuO2 loaded on carbon paper	1M KOH	CO	N.A.	Siritanaratkul et al.2023[15]
10	98	2.7	2.6	covalently grafted cobalt tetraaminophthalocyanine onto a positively charged polyfluorene backbone (PF-CoTAPc)/carbon	Nafion	Fumasep FBM	Ni Foam	1M KOH	CO	The catalyst was first soaked in 1M KOH followed by pure water	Li et al.2024[14]
25	101	3	2.8	covalently grafted cobalt tetraaminophthalocyanine onto a positively charged polyfluorene backbone (PF-CoTAPc)/carbon	Nafion	Fumasep FBM	Ni Foam	1M KOH	CO	The catalyst was first soaked in 1M KOH followed by pure water	Li et al.2024[14]
50	92	12	3	covalently grafted cobalt tetraaminophthalocyanine onto a positively charged polyfluorene backbone (PF-CoTAPc)/carbon	Nafion	Fumasep FBM	Ni Foam	1M KOH	CO	The catalyst was first soaked in 1M KOH followed by pure water	Li et al.2024[14]
75	85	17	3.2	covalently grafted cobalt tetraaminophthalocyanine onto a positively charged polyfluorene backbone (PF-CoTAPc)/carbon	Nafion	Fumasep FBM	Ni Foam	1M KOH	CO	The catalyst was first soaked in 1M KOH followed by pure water	Li et al.2024[14]
100	82	21	3.4	covalently grafted cobalt tetraaminophthalocyanine onto a positively charged polyfluorene backbone (PF-CoTAPc)/carbon	Nafion	Fumasep FBM	Ni Foam	1M KOH	CO	The catalyst was first soaked in 1M KOH followed by pure water	Li et al.2024[14]

|											
150	70	34	3.8	covalently grafted cobalt tetraaminophthalocyanine onto a positively charged polyfluorene backbone (PF-CoTAPc)/carbon	Nafion	Fumasep FBM	Ni Foam	1M KOH	CO	The catalyst was first soaked in 1M KOH followed by pure water	Li et al.2024[14]
200	56	43	4.1	covalently grafted cobalt tetraaminophthalocyanine onto a positively charged polyfluorene backbone (PF-CoTAPc)/carbon	Nafion	Fumasep FBM	Ni Foam	1M KOH	CO	The catalyst was first soaked in 1M KOH followed by pure water	Li et al.2024[14]
25	32	62	2.8	Mnbpy/MWCNT	Nafion	Fumasep FBM	RuO2 loaded on Ti	1M KOH	CO	N.A.	Eagle et al.2023[15]
50	33	70	3.2	Mnbpy/MWCNT	Nafion	Fumasep FBM	RuO2 loaded on Ti	1M KOH	CO	N.A.	Eagle et al.2023[15]
100	63	31	4	Mnbpy/MWCNT	Nafion	Fumasep FBM	RuO2 loaded on Ti	1M KOH	CO	N.A.	Eagle et al.2023[15]
50	69.7	32.631	2.9	NiNC-IMI	Sustainion	Fumasep FBM	Ni Foam	0.1M KOH	CO	N.A.	This work
100	63.4	31.73144	3.2	NiNC-IMI	Sustainion	Fumasep FBM	Ni Foam	0.1M KOH	CO	N.A.	This work
150	54.6	38.20403	3.4	NiNC-IMI	Sustainion	Fumasep FBM	Ni Foam	0.1M KOH	CO	N.A.	This work
200	45.4	44.59414	3.6	NiNC-IMI	Sustainion	Fumasep FBM	Ni Foam	0.1M KOH	CO	N.A.	This work
250	40.0	48.66628	3.8	NiNC-IMI	Sustainion	Fumasep FBM	Ni Foam	0.1M KOH	CO	N.A.	This work
300	35.2	52.4347	4.0	NiNC-IMI	Sustainion	Fumasep FBM	Ni Foam	0.1M KOH	CO	N.A.	This work
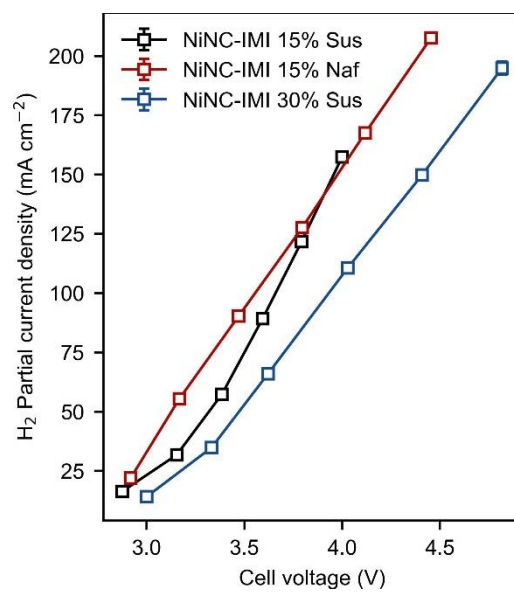
Fig. S6 Comparison of H$_2$ partial current densities against cell potentials between NiNC-IMI derived catalysts with 15% Sustainion, Nafion, and 30% Sustainion ionomers. The error bar represents the standard deviation of three tests.
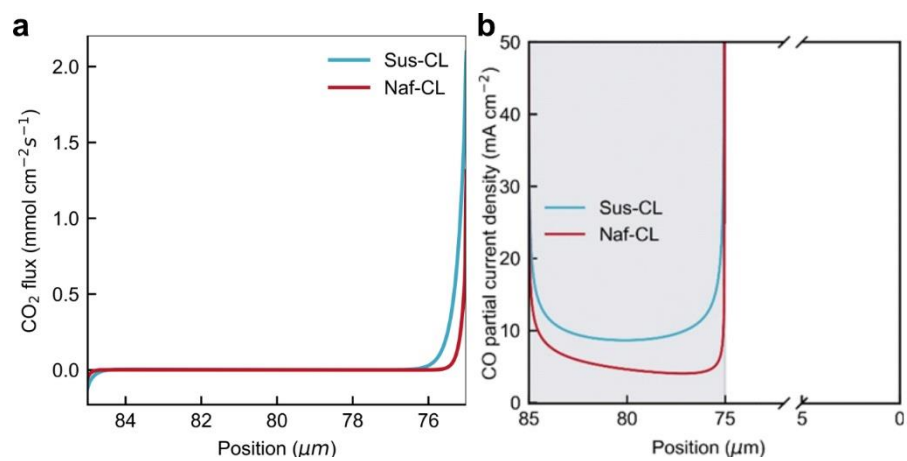
Fig. S7 Model predicted (a) CO₂ fluxes and (b) local partial current density of CO evolution within Sus- and Naf-CL.
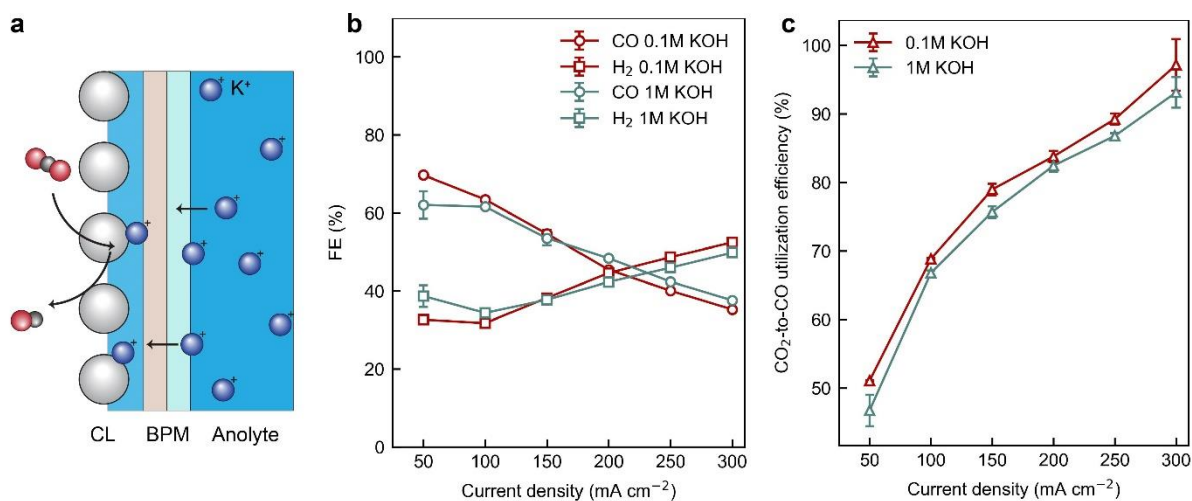
Fig. S8 BPMEA performance with varied anolyte concentration. (a) A schematic illustration of anolyte concentration effect on cation crossover. Comparison of the (b) CO Faradaic efficiency and (c) CO_2-to-CO utilization efficiency versus total current densities with 0.1 M or 1 M KOH aqueous anolyte. The BPMEA cell used cathodes with NiNC-IMI catalyst with 15% Sustainion ionomer as the catalyst layer. The error bar represents the standard deviation of three tests.
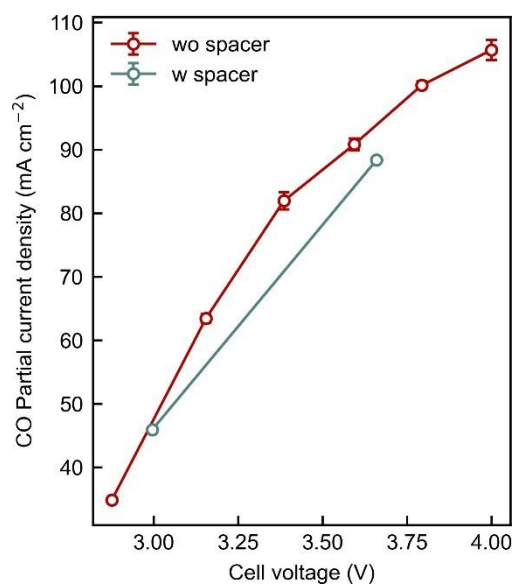
Fig. S9 Comparison of CO partial current density as a function of cell voltage for cells with and without spacer at between CL|CEL. The error bar represents the standard deviation of three tests.
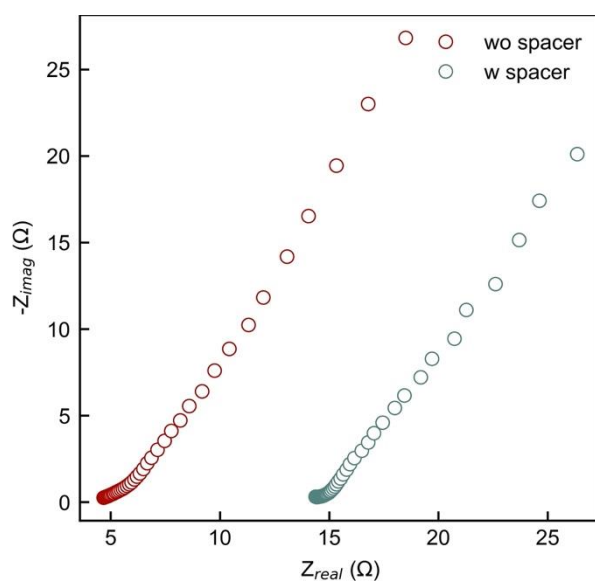
Fig. S10 Electrochemical impedance spectra of the BPMEA cells with and without spacer at open circuit voltage before CO$_2$ electrolysis conditioning.
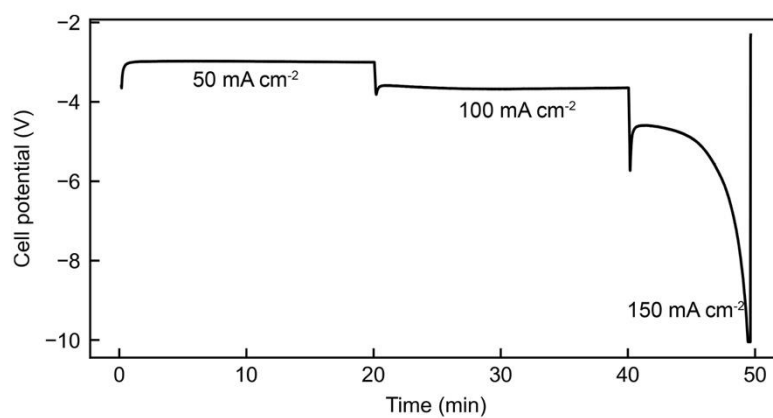
**Fig. S11 The cell overpotential overshoot for the BPMEA cell with the spacer at 150 mA cm⁻².**
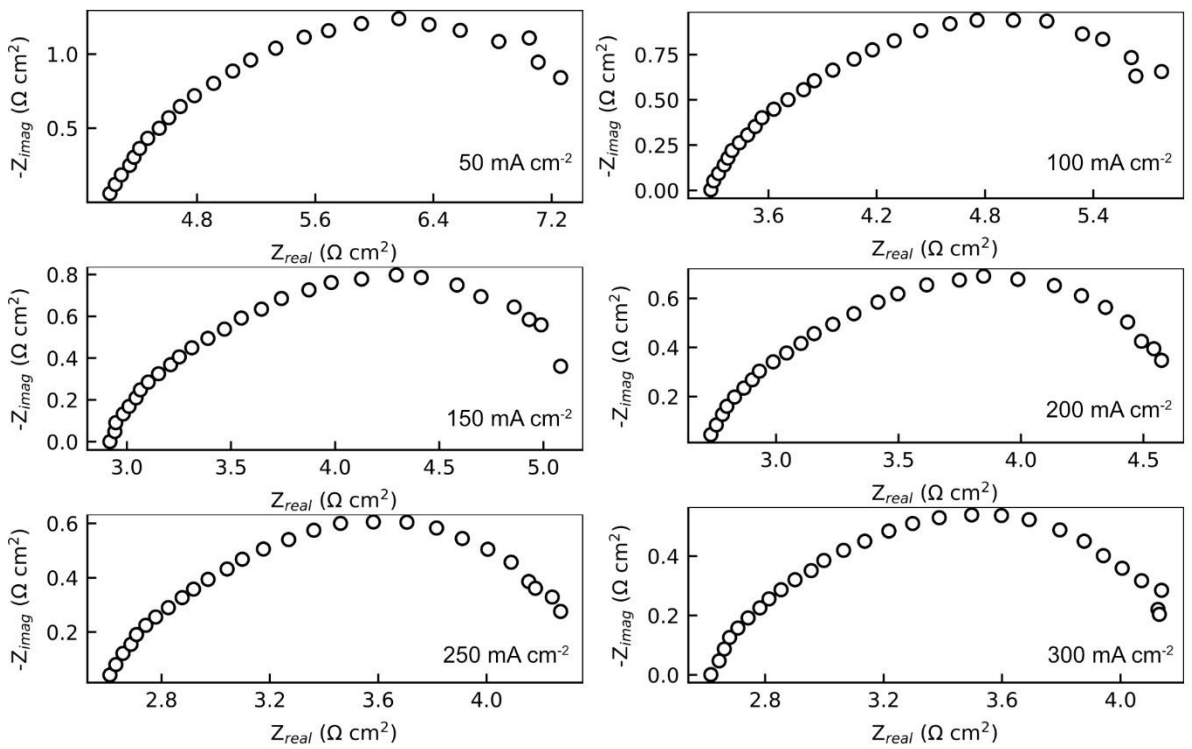
Fig. S12 Nyquist plots of electrochemical impedance spectroscopy for BPMEA with CL based with NiNC-IMI 15 wt% Sustainion ionomer as a function of current densities.
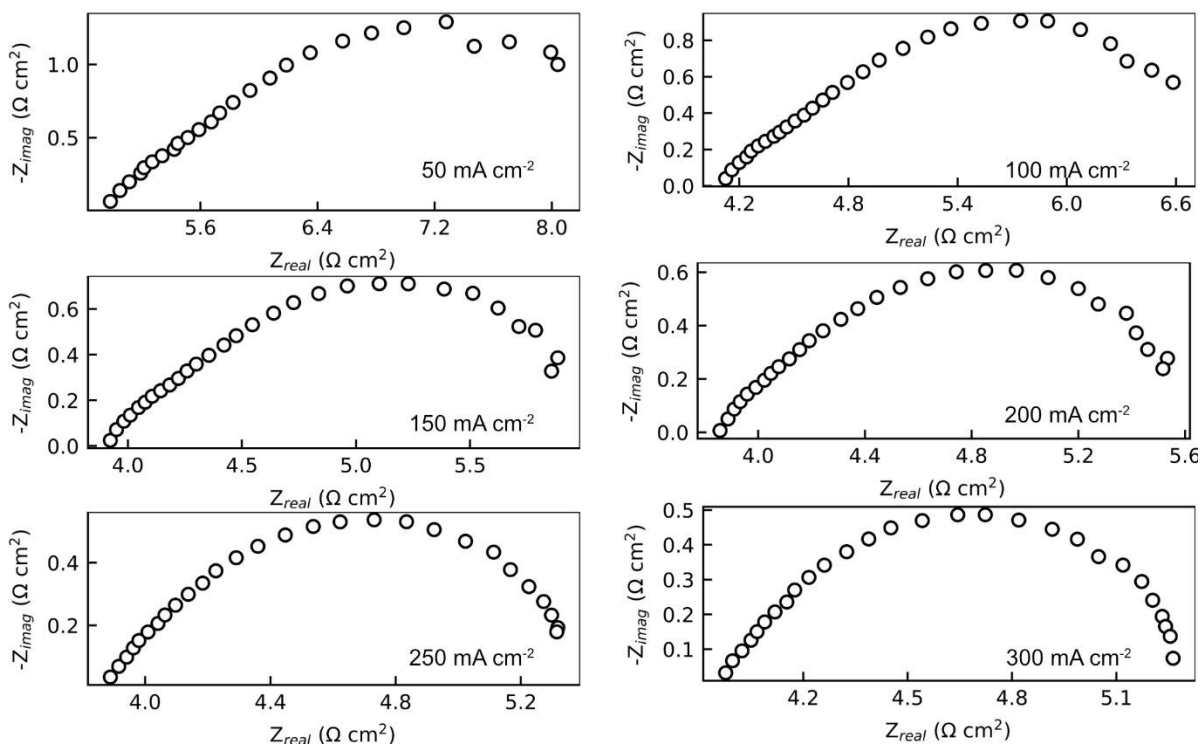
Fig. S13 Nyquist plots of electrochemical impedance spectroscopy for BPMEA with CL based with NiNC-IMI 15 wt% Naf as a function of current densities.
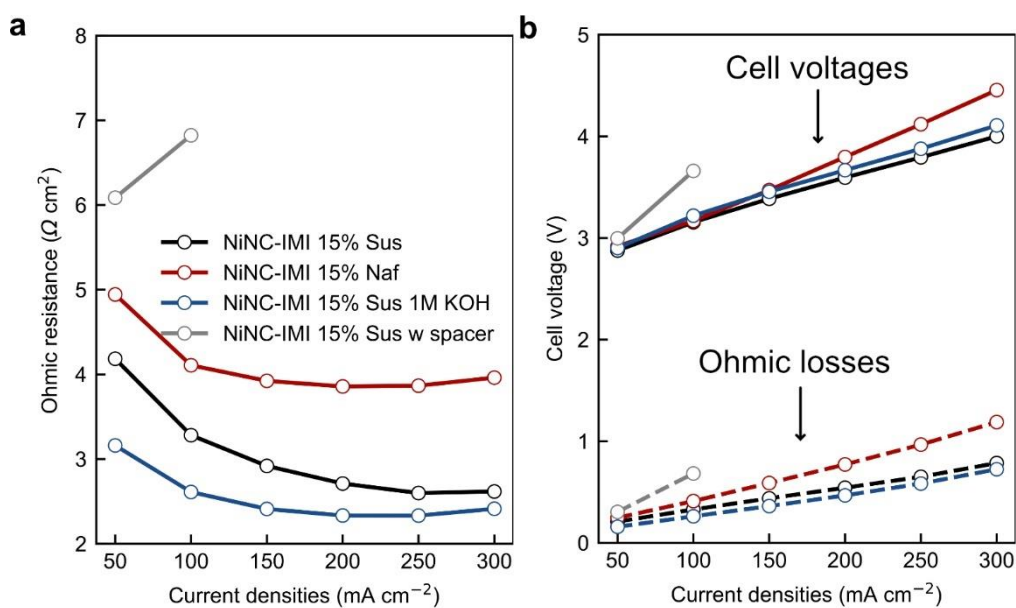
Fig. S14 Ohmic losses for BPMEAs. Comparison of (a) the ohmic resistances and (b) cell voltages (solid line) and ohmic losses (dashed lines) of the BPMEA as a function of current densities for CLs based with NiNC-IMI 15 wt% Sus, NiNC-IMI 15 wt%Naf, NiNC-IMI 15 wt% Sus using 1M KOH, and NiNC-IMI 15 wt% Sus with spacer at CEL|cathode interface. The rest of the samples used 0.1 M KOH as the anolyte.
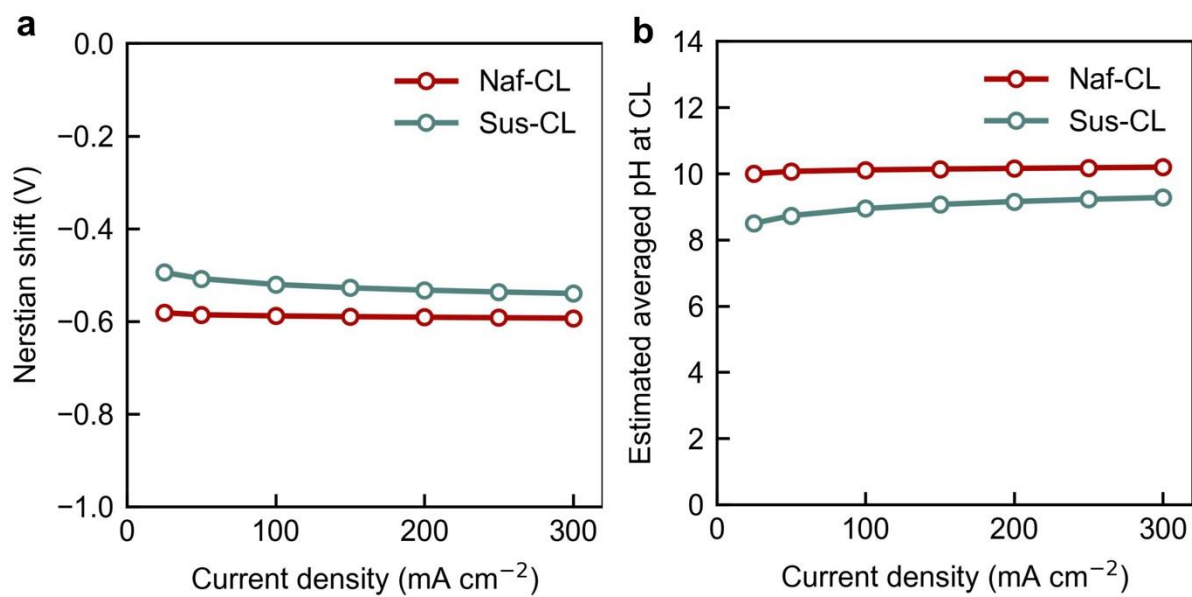
Fig. S15 Nernstian shifts for CL with different ionomers. Comparison of the (a)averaged Nernstian shift and (b) pH values caused by ionomers in the catalyst layers at different current densities estimated from models. Note: the more positive values of the Nernstian shift lead to reduced cell voltages.
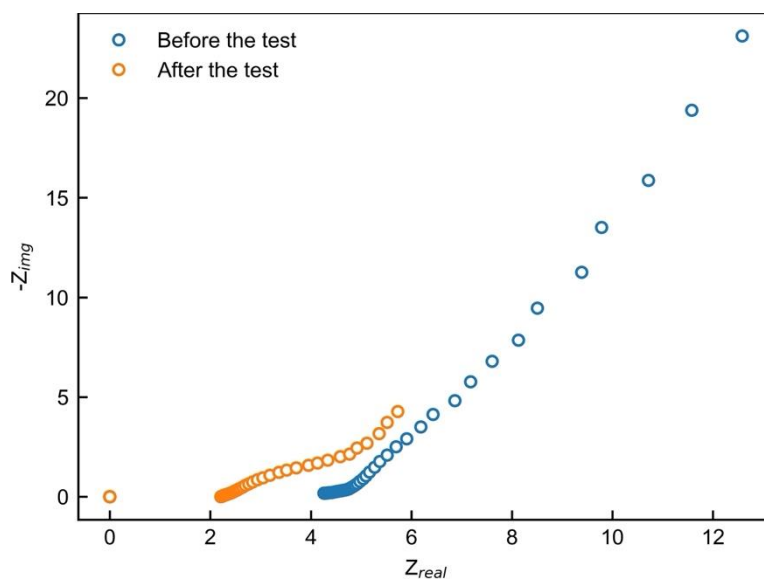
Fig. S16 Comparison of the electrochemical impedance analyses of the BPMEA cell at open circuit potential before and after the 150 h stability test.
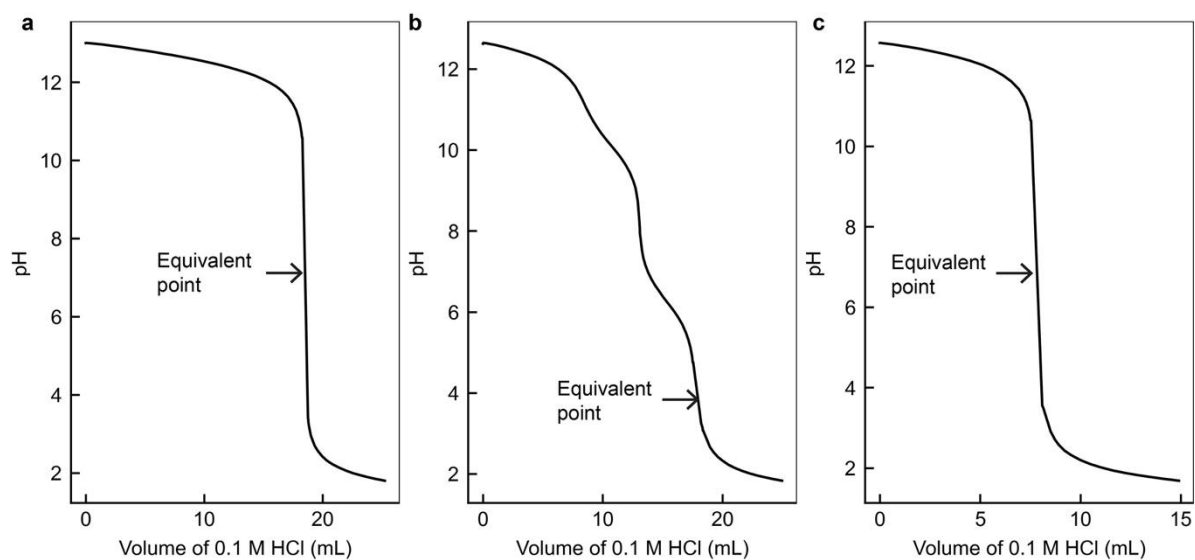
Fig. S17 Titration curves to determine averaged ion crossover. Examples of the titration curves for (a) fresh 0.1 M KOH anolyte, (b) anolyte after stability test, and (c) supernatant of the anolyte with excess BaCl₂ and carbonate removed after stability test.
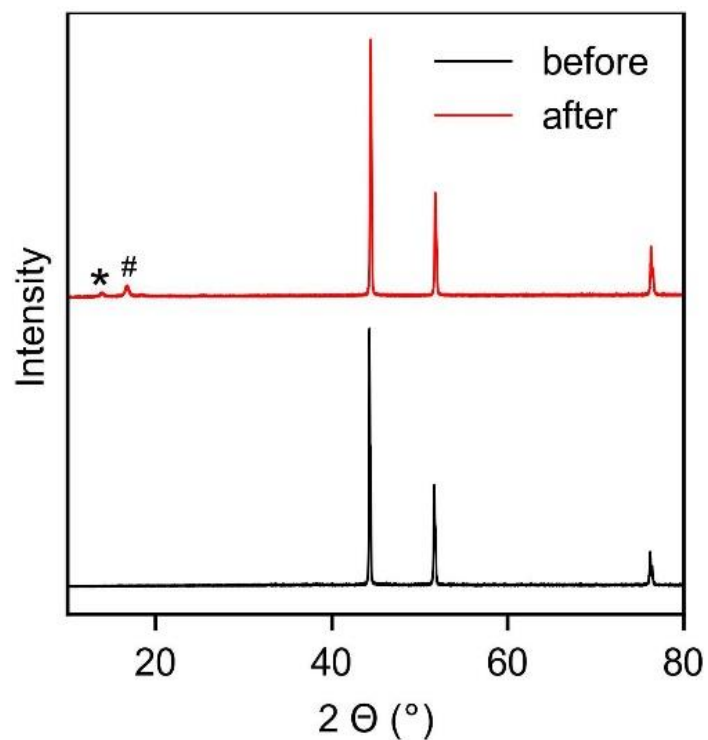
Fig. S18 Comparison of X-ray diffraction of the nickel mesh anode before and after 150 h stability test. The peak indicated by asterisk is related to the $K_{0.14}NiO_2$ phase (PDF 74-1792), and the peak highlighted by hashtag should be relevant to the phase similar to $K_9Ni_2O_7$ (PDF 71-1987).
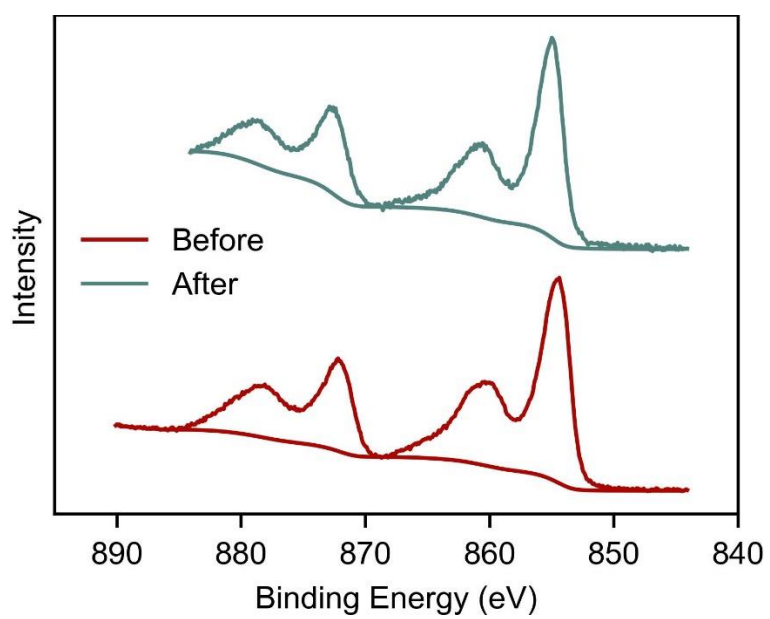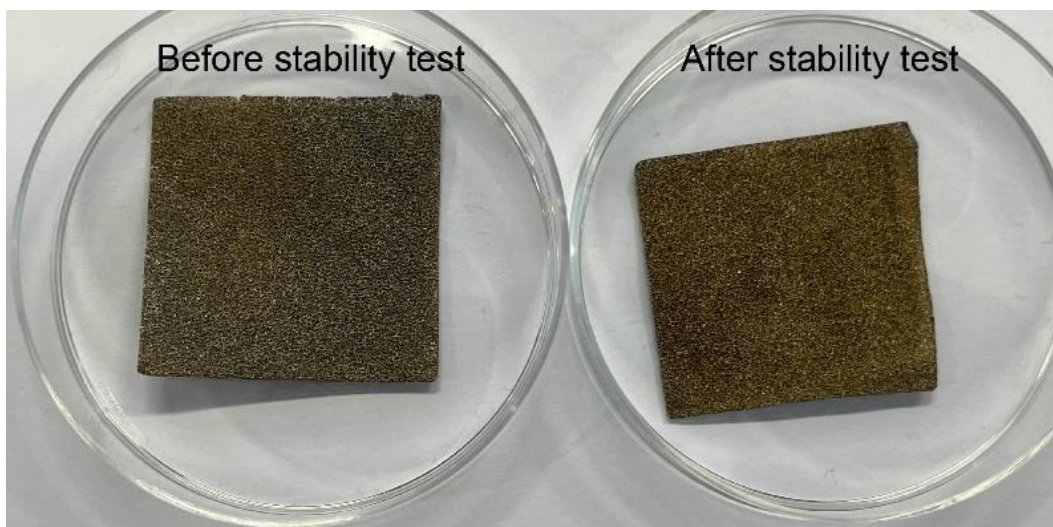
Fig. S19 X-ray photoelectron spectra of Ni 2p over the nickel mesh anode before and after 150 h stability test.
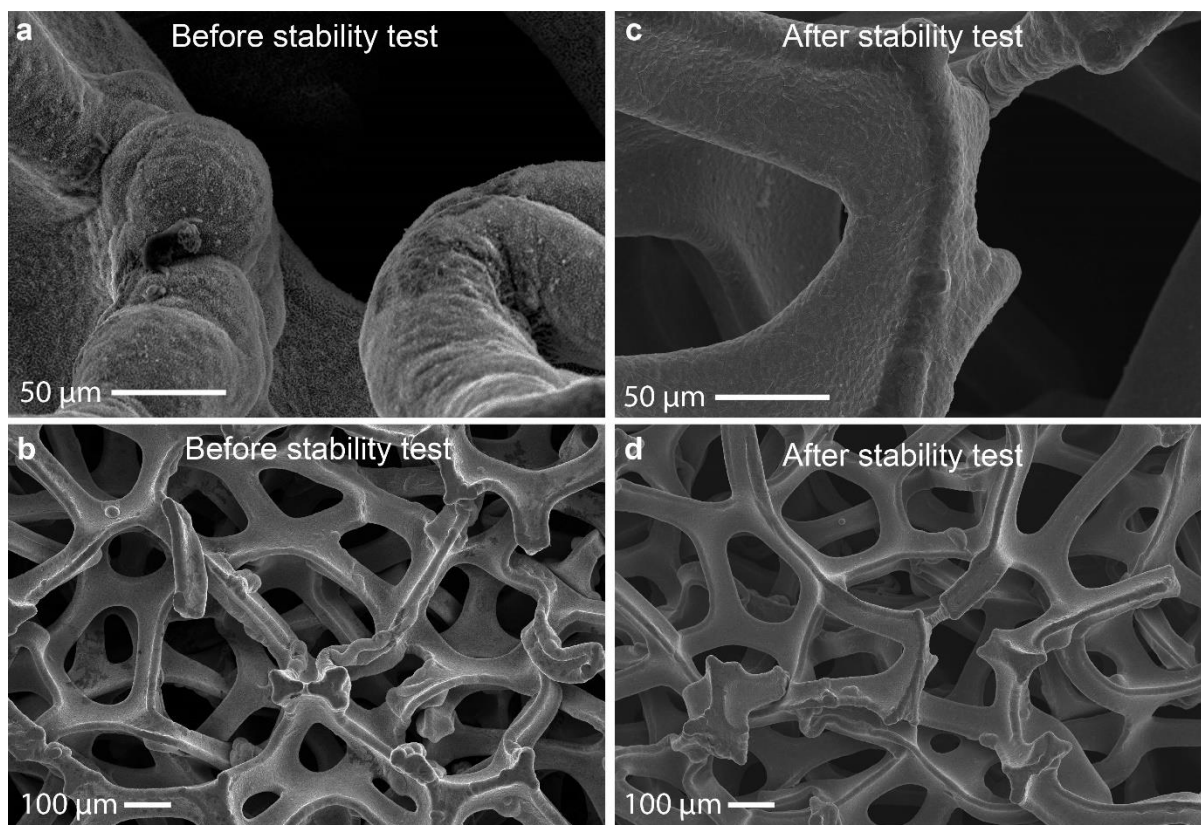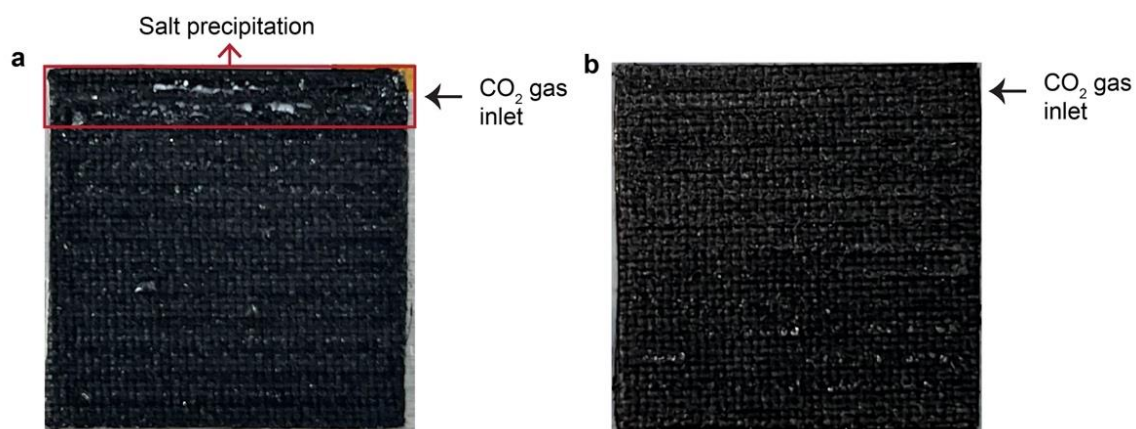
Fig. S20 Scanning electron micrographs of the nickel mesh anode surface microstructure (a, b) before and (c,d) after the stability test.

Fig. S21 Photos of the nickel mesh anode before and after the stability test.

Fig. S22 Images of the GDL side facing the CO$_2$ channels after (a) 40 h and (b) 150 h CO$_2$ electrolyses under 100 mA cm^{-2} with 1 L 0.1M KOH as the anolyte.

Supplementary References

1. Weng, L.-C., Bell, A. T. & Weber, A. Z. *Phys. Chem. Chem. Phys.* **2018**, *20* (25), 16973–16984.

2. Lees, E. W., Bui, J. C., Song, D., Weber, A. Z. & Berlinguette, C. P. *ACS Energy Lett.* **2022**, *7* (2), 834–842.

3. Zenyuk, I. V., Medici, E., Allen, J. & Weber, A. Z. *Int. J. Hydrog. Energy* **2015**, *40* (46), 16831–16845.

4. Weng, L.-C., Bell, A. T. & Weber, A. Z. *Energy Environ. Sci.* **2019**, *12* (6), 1950–1968.

5. Fuller, E. N., Schettler, P. D. & Giddings, J. Calvin. *Ind. Eng. Chem.* **1966**, *58* (5), 18–27.

6. Grew, K. N. & Chiu, W. K. S. *J. Electrochem. Soc.* **2010**, *157* (3), B327.

7. Bui, J. C., Digdaya, I., Xiang, C., Bell, A. T. & Weber, A. Z. *ACS Appl. Mater. Interfaces* **2020**, *12* (47), 52509–52526.

8. Luo, X., Kushner, D. I. & Kusoglu, A. *J. Membr. Sci.* **2023**, *685*, 121945.

9. Yang, K., Li, M., Subramanian, S., Blommaert, M. A., Smith, W. A., *et al. ACS Energy Lett.* **2021**, *6* (12), 4291–4298.

10. Siritanaratkul, B., Forster, M., Greenwell, F., Sharma, P. K., Yu, E. H., *et al. J. Am. Chem. Soc.* **2022**, *144* (17), 7551–7556.

11. Siritanaratkul, B., Sharma, P. K., Yu, E. H. & Cowan, A. J. *Adv. Mater. Interfaces* **2023**, *10* (15), 2300203.

12. Yue, P., Fu, Q., Li, J., Zhang, L., Ye, D., *et al. ACS Appl. Mater. Interfaces* **2023**, *15* (46), 53429–53435.

13. Xie, K., Miao, R. K., Ozden, A., Liu, S., Chen, Z., *et al. Nat. Commun.* **2022**, *13* (1), 3609.

14.   Li, G., Huang, L., Wei, C., Shen, H., Liu, Y., *et al. Angew. Chem. Int. Ed. n/a* (n/a), e202400414.

15.   Eagle, C., Neri, G., Piercy, V. L., Younis, K., Siritanaratkul, B., *et al. Sustain. Energy Fuels* **2023**, *7* (9), 2301–2307.